A glycan FRET assay for detection and characterization of catalytic antibodies to the *Cryptococcus neoformans* capsule

Conor J. Crawford[a,b,1], Maggie P. Wear[b], Daniel F. Q. Smith[b], Clotilde d'Errico[a], Scott A. McConnell[b], Arturo Casadevall[b,2,3], and Stefan Oscarson[a,2,3]

[a]Centre for Synthesis and Chemical Biology, University College Dublin, Dublin 4, Ireland; and [b]Department of Molecular Microbiology and Immunology, The Johns Hopkins Bloomberg School of Public Health, Baltimore, MD 21205

Edited by Dennis L. Kasper, Harvard Medical School, Boston, MA, and approved December 22, 2020 (received for review July 31, 2020)

Classic antibody functions include opsonization, complement activation, and enhancement of cellular antimicrobial function. Antibodies can also have catalytic activity, although the contribution of catalysis to their biological functions has been more difficult to establish. With the ubiquity of catalytic antibodies against glycans virtually unknown, we sought to advance this knowledge. The use of a glycan microarray allowed epitope mapping of several monoclonal antibodies (mAbs) against the capsule of *Cryptococcus neoformans*. From this, we designed and synthesized two glycan-based FRET probes, which we used to discover antibodies with innate glycosidase activity and analyze their enzyme kinetics, including mAb 2H1, the most efficient identified to date. The validity of the FRET assay was confirmed by demonstrating that the mAbs mediate glycosidase activity on intact cryptococcal capsules, as observed by a reduction in capsule diameter. Furthermore, the mAb 18B7, a glycosidase hydrolase, resulted in the appearance of reducing ends in the capsule as labeled by a hydroxylamine-armed fluorescent (HAAF) probe. Finally, we demonstrate that exposing *C. neoformans* cells to catalytic antibodies results in changes in complement deposition and increased phagocytosis by macrophages, suggesting that the antiphagocytic properties of the capsule have been impaired. Our results raise questions over the ubiquity of antibodies with catalytic activity against glycans and establish the utility of glycan-based FRET and HAAF probes as tools for investigating this activity.

glycans | glucuronoxylomannan | chemical biology | fungi | host–microbe interactions

Humans are protected from infectious diseases by physical defenses, endothermy, and an advanced immune system that includes both innate and adaptive arms (1). One of the remarkable aspects of adaptive immunity is the generation of specific antibodies (Abs) against microbial antigens, which aid the hosts immune defense against infection. Abs also serve as valuable research tools, diagnostics, and therapeutics (2). Furthermore, some Abs manifest catalytic activity to cleave antigens and possess intriguing innate capabilities, such as catalyzing the breakdown of oxygen into hydrogen peroxide (3–6). The existence of catalytic Abs was first hypothesized by the biochemist Jencks in the 1980s, using the framework of Pauling that if an Ab was raised against a transition state analog it could possibly cleave its substrate. Over the last three decades catalytic Abs have been an area of intensive research (7–9).

In an effort to develop therapies against *Cryptococcus neoformans*, an opportunistic fungus that is estimated to infect 1 million annually, with over 600,000 deaths (10), several glycoconjugate vaccine candidates were developed using synthetic and native polysaccharides based on the *C. neoformans* capsule (11–13). The capsule is composed of several constituents but the glucuronoxylomannan (GXM) dominates, accounting for 95% of capsule mass (14–16). Using hybridoma technology, monoclonal Abs (mAbs) have been developed against the GXM (2), with one Ab, 18B7, used in a phase I clinical trial as a candidate for passive antibody therapy for cryptococcal infections (17). In later years, this Ab and others were serendipitously discovered to have catalytic activity against peptide mimetics of the GXM; furthermore, indirect methods of analysis suggested glycosidase activity (4, 6). However, the lack of tools left many questions unanswered about their catalytic activity against their native glycan antigens.

The physiological roles of catalytic Abs in immunity are currently unresolved. For example, catalytic Abs are found in both patients with healthy outcomes and autoimmune conditions (18). One particular area where Ab catalysis may be relevant is in infectious diseases, as catalytic Abs could be effective, even if relatively slow, against microbial antigens since these infections often develop over a long time, which could permit even slow catalytic rates to have an effect (19). The prevalence of innate glycosidase activity in Abs is unknown and is particularly interesting when one considers the importance of Abs against bacterial polysaccharides in acquired immunity. Catalytic mAbs could work through cleaving immunosuppressive polysaccharide capsules, revealing more immunogenic epitopes to the immune

Significance

Cryptococcus neoformans is a global fungal pathogen that is a frequent cause of a life-threatening meningoencephalitis. There is a need for new therapies and vaccines. A better understanding of antibodies associated with its major virulence factor, the capsule, will allow the development of new antibody therapeutics, inform vaccine design, and further basic knowledge of antibody structure-function. Here, we demonstrate several antibodies against the capsule have innate glycosidase activity, and these antibodies can cause hydrolysis of the native capsule. This catalytic activity results in a disruption of cellular integrity and increased ease of phagocytosis by macrophages. To date, identifying this elusive quality in antibodies has been difficult. We have simplified this process by the development of a high-throughput FRET assay. This approach could be generalized to identify other antibodies catalytic against glycans.

Author contributions: C.J.C., M.P.W., A.C., and S.O. designed research; C.J.C., M.P.W., D.F.Q.S., C.d.'E., and S.A.M. performed research; C.J.C. and S.O. contributed new reagents/analytic tools; C.J.C., A.C., and S.O. analyzed data; and C.J.C., A.C., and S.O. wrote the paper.

The authors declare no competing interest.

This article is a PNAS Direct Submission.

[1]Present address: Department of Biomolecular Systems, Max Planck Institute of Colloids and Interfaces, 14476 Potsdam, Germany.

[2]A.C. and S.O. contributed equally to this work.

[3]To whom correspondence may be addressed. Email: acasade1@jhu.edu or stefan.oscarson@ucd.ie.

This article contains supporting information online at https://www.pnas.org/lookup/suppl/doi:10.1073/pnas.2016198118/-/DCSupplemental.

Published January 29, 2021.

system, aiding immune detection, and increasing the potency of Ab-dependent cellular cytotoxicity.

Herein, we report the design and synthesis of two glycan FRET probes to understand the prevalence of innate glycosidase activity in Abs against the cryptococcal capsule. To date, identifying this elusive quality in Abs was difficult to establish but we show through rational design of glycan-based FRET probes that glycosidase activity can be both identified and characterized. This approach could be generalized to identify other Abs catalytic against glycans. In our study, we highlight the enzymatic properties of four mAbs against the GXM, revealing intrinsic differences with regards to epitope specificity and isotype.

Results

Ab Epitope Mapping. Recently we have developed a synthetic glycan array containing a library of GXM structures (20). When screening this library with mAbs to *C. neoformans* GXM, we found a decasaccharide that was recognized by a wide variety of Abs (20). Consequently, we selected it as a good structure for the development into a FRET probe to serve as a potential assay to identify catalytic Abs. The synthesis of GXM related glycans are complicated by the presence of a 6-*O*-acetylation pattern. This *O*-acetylation is important for GXM Ab recognition but severely limits protecting group strategies (21, 22). To establish whether *O*-acetylation was important for oligosaccharide binding, we conducted a microarray study (Fig. 1*A*), which revealed that the binding to the nonacetylated decasaccharide was significantly diminished for mAb 18B7 and for all other mAbs screened binding was lost entirely (Fig. 1*A*). Consequently, we synthesized the more chemically challenging acetylated FRET probes.

Design and Synthesis of FRET Probes. We envisaged using the aminoalkyl linker present at the reducing end as a handle for the attachment of one-half of the FRET pair, then use another orthogonally protected amine at the nonreducing end, allowing selective attachment of the fluorophore and quencher, to access the desired glycan FRET probes (Fig. 2). Synthesis and assembly of the required building blocks for GXM assembly followed published protocols (20, 23–29). Through a convergent building block approach, we achieved the synthesis of the bifunctionally armed decasaccharide. Briefly, disaccharide acceptor **1** was coupled with thioglycoside donor **2** using DMTST in ether giving total 1,2-*trans* selectivity (30), following purification the 2-naphthylmethyl (NAP) ether was removed using oxidative conditions to yield tetrasaccharide acceptor **4** (Fig. 2*A*). This was then coupled with a glucuronic acid containing disaccharide **5** to give hexasaccharide **6**, solely as the α-anomer in 63% yield. Again, the orthogonal NAP group was chemoselectivity cleaved to access hexasaccharide acceptor **7**. The tetrasaccharide **8** was then assembled using inverse-glycosylation conditions as described by Guazzelli et al. (24), and the aminopropyl handle successfully attached to its free 3′-OH group under alkylating conditions, in the presence of the 6-*O*-acetyl group (→**9**, 70% isolated yield), with only minor de-acetylation occurring (8% of isolated yield) (Fig. 2*B*). Donor **9** was then used successfully in a coupling with acceptor **7** to create the *N*-orthogonally functionalized decasaccharide **10**, as the sole anomer in 85% yield. The *N*-phthalimido protecting group was then selectively removed in the presence of the 6-*O*-acetylation pattern using ethylenediamine, followed by formation of the *N*-Boc protected compound **11** in 57% yield. Decasaccharide **12** was then subject to palladium catalyzed hydrogenolysis, to remove benzyl protecting groups and reduce the linker azido group to an amine, using our developed optimized conditions, yielding **13** after P-2 size exclusion chromatography (Fig. 2*B*) (28, 31).

Subsequently, due to the limited quantity of material available, it was decided to telescope the final steps to minimalize the loss of material. First, the fluorophore was conjugated to the

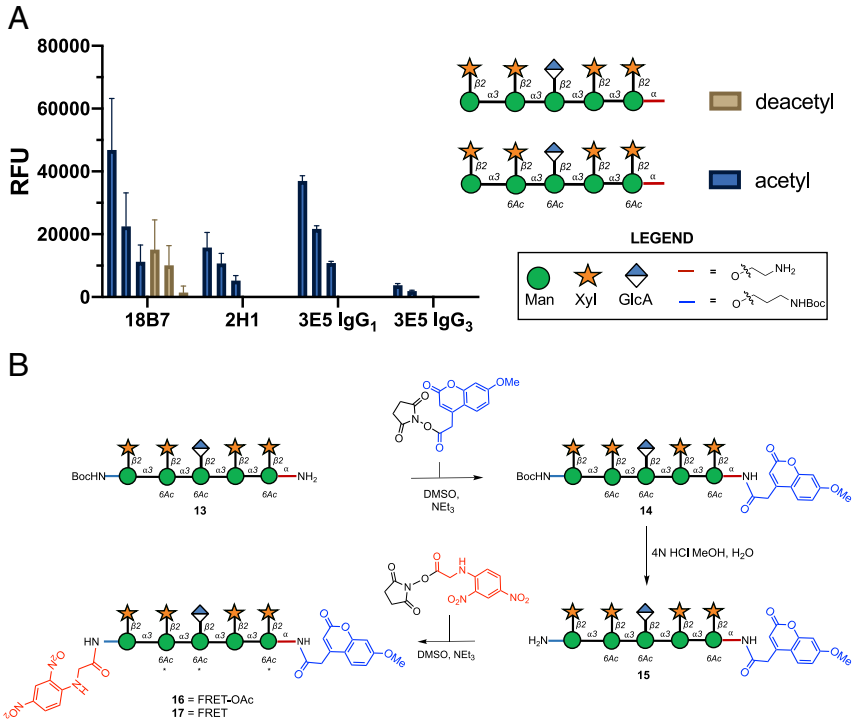

Fig. 1. Design and synthesis of glycan FRET probes. (*A*) Glycan microarray data showing Ab binding is affected by acetylation of GXM in a concentration-dependent manner (200 μM, 100 μM, 50 μM). Bars represent the mean ± SD. (*B*) Synthesis of two FRET probes. FRET-OAc **16** bears a 6-*O*-acetylation pattern, while FRET **17** in contrast bears no acetylation pattern (* = no 6-*O*Ac). Glycans are depicted according to symbol nomenclature for glycans (61).

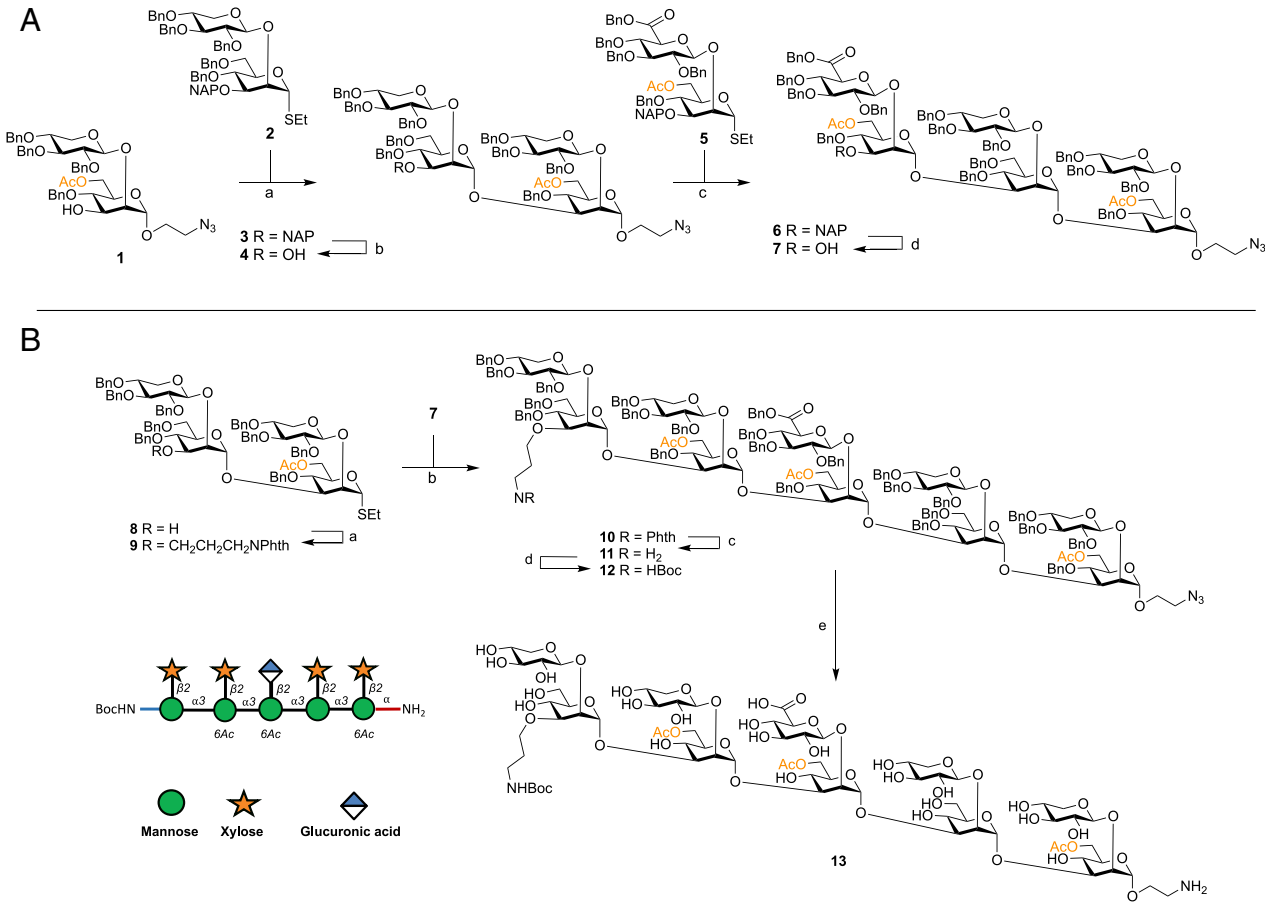

Fig. 2. Synthesis of bifunctionally armed oligosaccharide. (*A*) Reagents and conditions: (a) DMTST, Et_2O, 4 Å MS, 0 °C→room temperature, 80%; (b) DDQ, CH_2Cl_2:PBS (100 mM, pH 7.5) [85:15 (vol/vol)], 0 °C, 76%; (c) DMTST, Et_2O, 4 Å MS, 0 °C→room temperature, 65%; (d) DDQ, CH_2Cl_2:PBS (100 mM, pH 7.5) [85:15 (vol/vol)], 0 °C, 70%. (*B*) Reagents and conditions: (a) NaH 60% dispersion in mineral oil, DMF, 4 Å MS, $PhthNCH_2CH_2CH_2Br$, 0 °C→room temperature, 70%; (b) DMTST, Et_2O, 4 Å MS, 0 °C→room temperature, 85%; (c) ethylene diamine, *n*-BuOH, 90 °C; (d) Boc_2O, THF:H_2O [70:30 (vol/vol)], 57% two steps; (f) Pd/C (pretreated catalyst) (28), H_2, THF:^{t}BuOH:PBS (100 mM, pH 5) [60:10:30 (vol/vol/v)], 66%.

amino linker using an *N*-hydroxysuccinimide (NHS) active ester of 7-methoxycoumarin-4-acetic acid (MCA), to produce compound **14** (Fig. 1*B*). Subsequently, the *N*-Boc group was removed using an aqueous mixture of 3 M HCl methanol to produce **15**. The final conjugation was carried out using the NHS-activated *N*-(2,4-dinitrophenyl) glycine (DNP) to give 5.4 mg of the target desired FRET probe **16** in 56% overall yield over the three steps. Despite the initial evidence that nonacetylated structures are poorly recognized in the microarray assay (Fig. 1*A*), we decided to further investigate the importance of the 6-*O*-acetylation pattern in the Ab recognition and possible catalysis in solution. Deacetylation of a portion of the decasaccharide FRET-OAc probe under basic conditions yielded 2 mg of FRET probe **17**. The two probes are termed FRET-OAc (**16**), for the decasaccharide with acetyl groups, and FRET (**17**) for the nonacetylated decasaccharide.

A FRET Assay to Detect Catalytic Abs. Four murine monoclonal Abs were investigated: 18B7 (IgG_1), 2H1 (IgG_1) (32), and two isotypes of 3E5, one IgG_1 and one IgG_3, which have identical variable regions but differ in the constant region (33). mAbs 2H1, 18B7, and 3E5 (IgG_3) were generated from B cells harvested from the spleen on mice immunized with a GXM-tetanus toxoid conjugate vaccine (21), while mAb 3E5 (IgG_1) was generated by in vitro isotype switching. Each of these mAbs bind to the GXM capsular polysaccharide of *C. neoformans*. mAbs 18B7 and two 3E5 isotypes (IgE and IgA) were previously shown to catalyze cleavage of a peptide mimetic of the GXM, termed P1 (SPNQHTPPWMLK) (4, 5). To determine if this activity extended to the oligosaccharide binding targets, mAbs 18B7, 3E5 (IgG_1), 3E5 (IgG_3) (800 μg/mL), and 2H1 (580 μg/mL) were incubated with 400 μM of either the oligosaccharide FRET-OAc or FRET probe in a fluorescence spectrometer (λ_{ex} 320 nm λ_{em} 405 nm) at 37 °C for 70 h (Fig. 3). mAb 18B7 showed moderate catalytic activity toward both FRET probes, while mAb 3E5 (IgG_1) displayed comparable results to mAb 18B7 when incubated with both FRET probes. Interestingly, the IgG_3 variant of 3E5 differed in specificity toward the two FRET probes when compared to 3E5 (IgG_1), despite having the same variable sequence. In contrast to the IgG_1 variant, 3E5 (IgG_3) displayed no catalytic activity toward the FRET probe but showed the second highest efficiency in cleaving the FRET-OAc probe. mAb 2H1 caused the greatest cleavage of the FRET-OAc probe, while showing similar levels of low activity toward the FRET probe as mAbs 18B7 and 3E5 (IgG_1) (Fig. 3).

Michaelis–Menten Kinetics of Abs with Catalytic Against Glycans. Next, we sought to determine the Michaelis–Menten (MM) kinetics of mAbs against both FRET probes. To investigate, we incubated both Abs with varying concentrations of the FRET probes **16** or **17** and plotted the change in velocity (V_0) as a function of substrate concentration (Table 1 and *SI Appendix*, Fig. S4). In the case of mAb 3E5-IgG_3, no breakdown was observed, mirroring the assay result, meaning we were unable to determine its MM

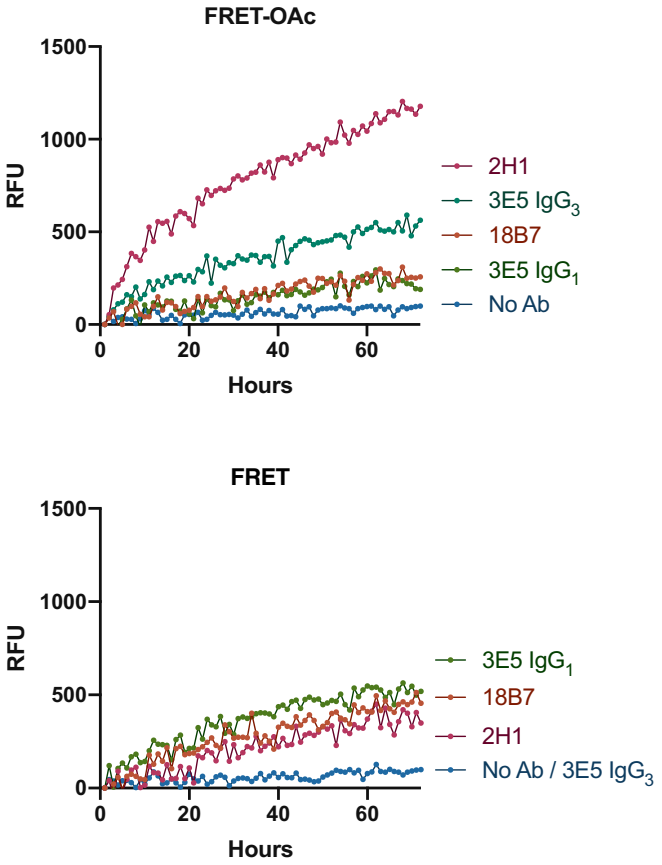

Fig. 3. A glycan-based FRET assay to detect catalytic Abs.

kinetics toward the deacetylated FRET probe. This was not the case for isotype switch variant mAb 3E5-IgG$_1$, thus by virtue of 3E5-IgG$_3$ mAbs lack of activity, we note that mAb 3E5-IgG$_1$ was superior at breakdown of the FRET probe (Table 1, entries 3 and 4). In the case of FRET-OAc, we managed to determine the kinetics for both 3E5 mAbs (Table 1, entries 7 and 8). Comparison of the two 3E5 isotype variants revealed they have similar K_m values but mAb 3E5-IgG$_3$ presented to have a higher turnover number (k_{cat}), meaning it had a higher catalytic efficiency toward the FRET-OAc probe (Table 1, entries 7 and 8).

The MM kinetics of mAb 18B7 against the P1 peptide has been described by Bowen et al. (4). While the K_m of mAb 18B7 toward the P1q FRET peptide ranged from 46 to 55 μM, our results showed mAb 18B7 has much lower K_m for the glycan substrate compared to the peptide. This is not surprising, given that this Ab was raised against the polysaccharide capsule. The k_{cat} values of mAb 18B7's cleavage of the FRET probes was also at least twofold of that measured for mAb 18B7s cleavage of the P1q peptide (FRET peptide, 1×10^{-2} μM^{-1}/s^{-1}).

For mAb 2H1, we were able to calculate the MM kinetic parameters for mAb 2H1 against both FRET probes (Table 1, entries 2 and 6). mAb 2H1 had a lower K_m for the acetylated FRET probe and overall a higher catalytic efficiency toward the breakdown of the FRET-OAc probe (Table 1, entries 2 and 6). Overall, when comparing each mAb's catalytic efficiency toward both FRET probes, it was clear mAb 2H1 was most the efficient at cleaving both the FRET and FRET-OAc probes; therefore, we focused the rest of our investigation on mAb 2H1 to hopefully gain insights into the most efficient Ab identified to date with innate catalytic activity against glycans.

Ab 2H1 Has Peptidase Activity. The GXM mimetic, P1 (SPNQHTPPWMLK) (4, 5) when incubated with mAb 2H1 at 37 °C resulted in cleavage of the P1 peptide, as was suggested by the disappearance of the parent material ion 1,435.7 *m/z*, and the appearance of fragment ions (*SI Appendix*, Fig. S2). In particular, the ion 690.9 *m/z* corresponded to cleavage between threonine and proline (SPNQHT/PPWMLK) but it was not possible to identify the other half of this fragment at 769.4 *m/z* (PPWMLK). This suggests mAb 2H1 causes cleavage between the same residues as mAb 18B7 (threonine and proline) but differed to the cleavage pattern of the 3E5 Abs (SPNQHTPPWM/LK) (4). Next, we used a P1q FRET (200 μM) peptide recently described by Bowen et al. (4), which confirmed that 2H1 (375 μg/mL) had enzymatic activity toward the peptide probe but at much lower levels than 18B7 (*SI Appendix*, Fig. S1 *C* and *D*).

Ab 2H1 Is a GXM Lyase. To gain understanding of how the Abs were breaking down GXM, we incubated mAbs 2H1 and 18B7 with a synthetic oligosaccharide for 2 d at 37 °C (Fig. 1, acetylated decasaccharide). Mass spectrometry analysis of how mAb 18B7 hydrolyses the GXM was reported previously (4), and was again confirmed by our experiments finding an ion corresponding to a hexasaccharide (1,116.0 *m/z*) (*SI Appendix*, Fig. S9), suggesting cleavage along the mannose backbone, specifically between third and fourth mannose from the reducing terminus, representing an endoglycosidase-like activity.

In the mAb 2H1 incubation, breakdown was suggested by disappearance of the parent ion and the appearance of fragments; initially we sought to identify the products of hydrolysis but were unable to do so. Noting that polysaccharide breakdown can also occur through more unconventional mechanisms (34), such as those of polysaccharide lyases (35), prompted us to wonder if mAb 2H1 proceeded through this mechanism. Further analysis of the mass spectra allowed the successful identification of the 1,2-enol ether breakdown products (*SI Appendix*, Fig. S10) (34, 35). Two distinct cleavage products were identified, which corresponded to cleavage along the mannose backbone either side of the internal β-1,2 glucuronic acid mannose disaccharide moiety, with the presence of the distinctive enol ether fragments confirmed. Overall, our results and previous mass spectrometry analysis of 18B7 (4), suggest that mAbs 18B7 and 2H1 operates through enzymatically distinctive mechanisms for GXM breakdown.

Absence of Classic Catalytic Residues in 2H1 Paratope. The proteolytic catalytic activity of mAb 18B7 was recently studied in detail and catalytic residues were proposed (4); however, a crystal structure for 18B7 does not yet exist. In contrast, a crystal structure of the fragment antigen-binding (Fab) domain of mAb 2H1 bound to a peptide mimetic of GXM was solved by Young et al. (36) (Fig. 4*B*). Using the PDB file and the open-access

Table 1. MM kinetics of catalytic Abs

Entry	Antibody	FRET probe	K_m (μM)	k_{cat} (s^{-1})	k_{cat}/K_m (μM^{-1}/s^{-1})
1	18B7	FRET	35.8×10^{-3}	26.4×10^{-3}	7.3×10^{-1}
2	2H1	FRET	54.7×10^{-3}	$42.6 \times 10\text{-}3$	7.7×10^{-1}
3	3E5-IgG$_1$	FRET	55.7×10^{-3}	27.5×10^{-3}	7.4×10^{-1}
4	3E5-IgG$_3$	FRET	ND	ND	ND
5	18B7	FRET-OAc	48.3×10^{-3}	25.7×10^{-3}	5.3×10^{-1}
6	2H1	FRET-OAc	36.3×10^{-3}	33.5×10^{-3}	9.2×10^{-1}
7	3E5-IgG$_1$	FRET-OAc	35.9×10^{-3}	26.7×10^{-3}	4.9×10^{-1}
8	3E5-IgG$_3$	FRET-OAc	35.0×10^{-3}	29.0×10^{-3}	8.2×10^{-1}

The initial velocity (V_0) of each reaction was determined and plotted as a function of substrate concentration, the data were fit to the MM equation for a single-step bimolecular reaction using nonlinear regression. K_m and k_{cat} were calculated using Prism 8. ND, not determined. Each experiment was repeated in triplicate.

modeling server GLYCAM (37–39), we performed Ab docking studies to determine the glycan–Ab interactions for 2H1 (Figs. 4*A* and 5). We performed docking studies with both acetylated (*SI Appendix*, Fig. S6) and deacetylated (Fig. 4) GXM structures, with the highest-scoring binding affinities predicted to be −10 kcal/mol for both acetylated and deacetylated structures. When we applied an adaptive Poisson–Boltzmann solver to the 2H1 Fab, it revealed an electropositive cleft (Fig. 4*B*). Considering that GXM is an anionic polysaccharide, this electropositive cleft suggests a role for ionic interactions in affinity between the Ab and antigen. The highest-scoring docked structures predict that the carboxylic acid moiety of glucuronic acid residue engaging in hydrogen bonding with asparagine residue 33 (approximately 3 Å) (Fig. 5). The importance of xylose side-chains was also apparent by the modeling results with the highest scoring docking structures having xylose branches in pockets underneath tyrosine and phenylalanine residues, possibly being stabilized by CH/π stacking (Fig. 5) (40). We also sought through modeling to discern the residues responsible for catalysis, and while no definitive assignment was possible, it was clear that no classic catalytic residues were present in the antigen binding site (e.g., two carboxyl groups 5 to 10 Å apart) (41), or those that have been observed for sialidases (42). The classic Ser-His-Asp catalytic triad, that was proposed by Bowen et al. (4) to be responsible for the cleavage of the P1 peptide by 18B7 was also absent from mAb 2H1. Despite the absence of conventional glycosidase motifs, there was an abundance of nucleophilic amino acids tyrosine, histidine, and asparagine, which could work in tandem to produce acid-base catalysis to promote the observed glycosidase activity. In future work mutagenesis experiments will be required in order to determine the residues responsible for catalysis.

GXM Secondary Structure. Using GLYCAM carbohydrate builder, we predicted the conformations of acetylated and nonacetylated decasaccharide, to try and better understand this phenomenon (37–39). In both models GXM adopts a helical conformation due to the α-mannose backbone, that is decorated by branching of β-xylose and β-glucuronic acid residues (Fig. 4*C*). Molecular modeling predicts that the mannan backbone conformation is not altered by acetylation of GXM (*SI Appendix*, Fig. S5). However, acetylation does create new epitopes and a hydrophobic substituent, which may allow increased Ab binding, which could explain the differences observed for acetylated and nonacetylated structures. When performing GXM modeling and Ab–antigen docking experiments, it became apparent that the P1 peptide and decasaccharide both adopted a helical conformation, both bound to the same binding site, making the peptide a "mimotope," mimics of epitopes, something previously hypothesized and experimentally demonstrated previously through ELISA (Fig. 4*C* and *SI Appendix*, Fig. S1 *A* and *B*) (4–6).

Catalytic Abs Perturb Capsule and Cellular Integrity. To discern if the glycosidase activity on the FRET probes was predictive of activity on the native capsule, we incubated cells with 10 μg/mL of mAbs 2H1, 18B7, control IgG or no Ab for a week with heat killed H99 *C. neoformans* cells, at 30 °C with agitation. After a week, the capsule diameter was not altered in the absence of Ab or after incubation with the control IgG_1 Ab. In contrast, cells incubated with mAbs 2H1 or 18B7 showed a significant decrease in mean capsule diameter ($P < 0.0001$). The reduced capsule diameter could suggest capsule breakdown through a glycosidase mechanism. We also observed a population of cells incubated with either 18B7 or 2H1 had lost the majority of their capsule (Fig. 6 *A* and *B*), possibly indicating capsular heterogeneity, and differing susceptibility to Ab-mediated catalysis, even when using the same strains, under the same growth conditions (4, 14, 16).

Next, we sought to determine whether the observation of the decrease in capsule diameter was the result of glycosidase activity on the GXM. To do so we devised an experiment using the

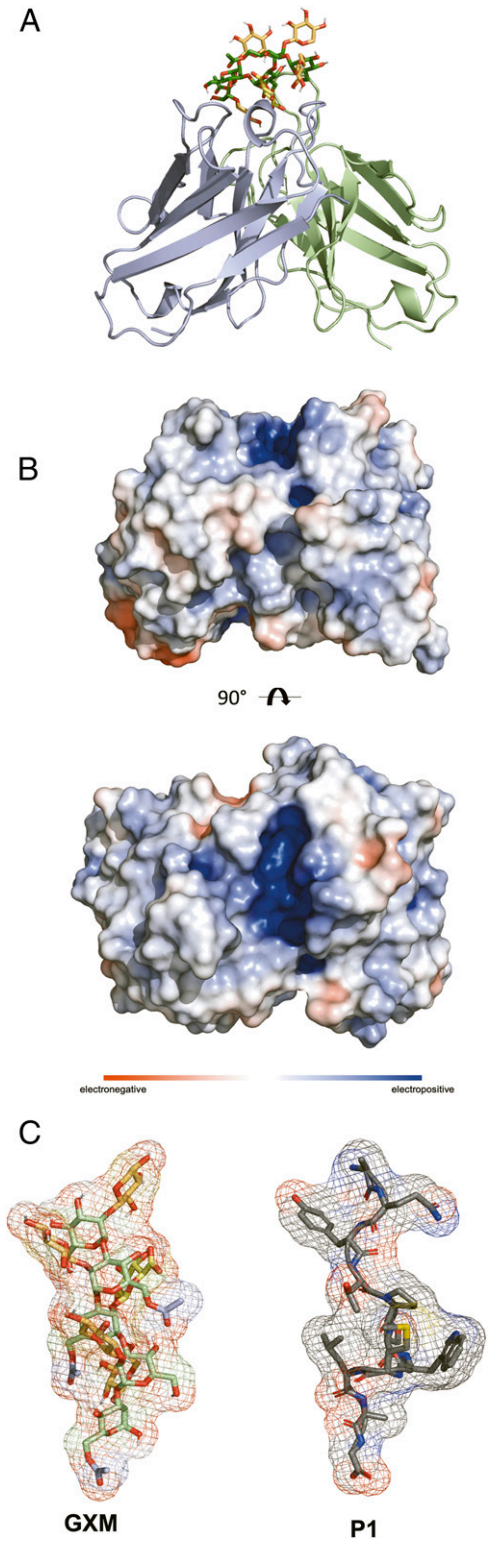

Fig. 4. Crystal structure of 2H1 and GXM peptide mimotope P1 and molecular docking studies with GXM. (*A*) Crystal structure of anti-GXM mAb 2H1. VH shown in light blue and VL light chain shown in pale green with docked GXM. (*B*) Calculated electrostatic surface potential of 2H1. Electrostatic surface potentials are colored red for negative charges, blue for positive charges, and white color represents neutral residues. Electrostatic surface potential was calculated using adaptive Poisson–Boltzmann solve in PyMOL. mAb 2H1 shows a positively charged cleft (+10 kT to −10 kT). (*C*) GXM and P1 both adopt a helical conformation. Glycam Carbohydrate Builder was used to construct the ligand.

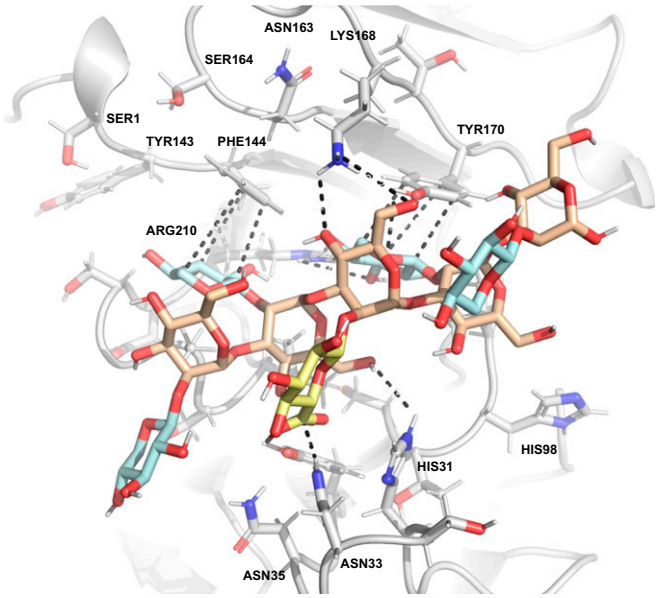

Fig. 5. Absence of classic catalytic residues in 2H1 paratope. Hydrogen bonding interaction between 2H1 mAb and decasaccharide.

hydroxylamine-armed fluorescent (HAAF) probe that we recently used to explore the architecture of the *C. neoformans* capsule (43). That study was remarkable in that reducing ends were only visualized at the cell wall–capsule interface and not within the capsule body itself. We reasoned that if the mAbs were hydrolyzing capsular GXM, we may see the appearance of HAAF probe-related staining extracellularly or in the capsule body. To examine this, we incubated catalytic Abs 2H1 and 18B7, a control mAb, and no mAb, with heat-killed *C. neoformans* cells. After 3 and 7 d cells were visualized through fluorescence microscopy, using fluorescent anti-IgG secondary Abs (red), and a HAAF probe (green) (43). On day 3, no staining of the hydroxylamine probe occurred in the capsule (*SI Appendix*, Figs. S7 and S8). However, on day 7, we observed the appearance of HAAF probe related staining in the capsule of 18B7 but none in mAb 2H1 or in controls (Fig. 6*C*). The absence of staining in the 2H1 mAb incubation was further evidence of its lyase activity. As by virtue of the HAAF probes mechanism, it will only stain reducing end glycans and not label the enol ether related breakdown products of 2H1.

Catalytic Abs Alter Complement Deposition and Enhance Phagocytosis by Macrophages. To investigate if there was any biological significance to mAb 2H1-mediated catalytic activity on the cryptococcal capsule, we removed the Ab after 7 d of incubation (gentle elution buffer, pH 6.6) from the cells and added C3 complement. Previously, complement has been shown to bind to the capsule of H99 cells in an annular pattern, ultimately resulting in enhanced Ab-mediated phagocytosis (44). Conversely, H99 cells incubated with mAb 2H1 for 7 d had highly localized complement deposition on the cell surface (Fig. 7*A*), suggesting the catalytic Ab changes the structure of the capsule which is visualized by alteration in complement binding to the capsule. To test if this altered complement deposition resulted in changes in phagocytosis, we studied fungal cell uptake by bone marrow-derived macrophages (BMDMs) measuring the phagocytic index. *C. neoformans* cells treated with mAb 2H1 followed by its removal were more efficiently ingested than nontreated cells, suggesting that Ab-mediated catalysis had altered the structure of the capsule, reducing its antiphagocytic properties ($^{***}P \leq 0.001$) compared to untreated cells (Fig. 7*B*) (30.5% vs. 19.8%). Catalytic Ab-treated cells had comparable levels of phagocytosis (37.1%) to cells treated with Abs and complement alone (36.6%), suggesting the antiphagocytotic properties of the capsule were reduced such that macrophages ingested them to a level similar to the presence of complement alone. Phagocytosis could again be further increased by the addition of complement to Ab-treated cells (46.6%), suggesting a synergistic benefit when used in combination (Fig. 7*B*).

Discussion

Here we report the design and synthesis of two glycan-based FRET probes, which, compared to their peptide counterparts, are significantly underdeveloped, having only a handful of literature reports (45–50). To our knowledge, this example of glycan-based FRET probes being used to resolve the kinetics of catalytic Abs is unique. Glycan FRET probes may find further utility in helping to characterize carbohydrate active enzymes (CAZy), and catalytic Abs against glycans.

The glycan FRET probes used here establish that a number of Abs against the cryptococcal capsule have innate glycosidase activity. Notably some mAbs displayed no activity toward one FRET probe but had activity toward the other (e.g., 3E5 IgG_3); differences between the IgG_1 and IgG_3 mAb variants likely reflect constant region constraints on the IgG paratope that affect enzymatic activity. While the importance of GXM acetylation for Ab binding is noted in the literature, we observed some distinct differences in binding between the microarray binding study (Fig. 1) and FRET probes. Neither mAb 2H1 nor 3E5 (IgG_1) bound to the deacetylated decasaccharide on the microarray but displayed glycosidase activity to the deacetylated FRET probe. There are two interpretations of this result: One is that the interactions between the nonacetylated GXM and the mAb is more transient meaning that microarrays cannot reliably detect weaker glycan–protein interactions; the other is that the addition of the aromatic and hydrophobic FRET pair affects the Ab–glycan interactions and may explain the enzymatic activity to the nonacetylated FRET probes.

In the microarray study we demonstrated the importance of acetylation on the molecular level for Ab recognition of GXM (Fig. 1*A*). Molecular modeling predicts no change in conformation due to acetylation, but does create new epitopes, which may be important for Ab binding by creating hydrophobic pockets to which an Ab can bind, something supported by more complex modeling, recently completed in collaboration with Kuttell et al. (51). Recently, we also observed differences in cell surface hydrophobicity between serotypes of *C. neoformans*, which could be accounted for by differences in acetylation of GXM (52).

Previously, we reported that isotype switching 3E5 (IgG_3) to 3E5 (IgG_1) resulted in turning a nonprotective Ab to a protective Ab (33). Although these differences were largely attributed to differences in constant region engagement of Fc receptors, the glycan microarray study visualized a difference in relative fluorescence units (RFU) between the two isotypes to acetylated decasaccharide (Fig. 1*A*). The greater RFU observed suggests 3E5 (IgG_1) is able to bind with far greater affinity to GXM, and this may also contribute to the observed differences in efficacy of the two Abs in vivo. mAb 18B7 further followed this observed trend with similar levels of binding signal to the acetylated decasaccharide. Protective mAb 2H1 also displayed higher RFU to the acetylated decasaccharide than the nonprotective 3E5 (IgG_3), which suggests there is a correlation between RFU for an epitope, and a mAb with protective efficacy. In the microarray study, it was also obvious that the mAbs had a "preference" for acetylated structures, giving insight into the mammalian immune response against cryptococcal infections, suggesting a bias or competitive advantage for Abs that recognize acetylated structures. Differences in Ab binding could originate during somatic

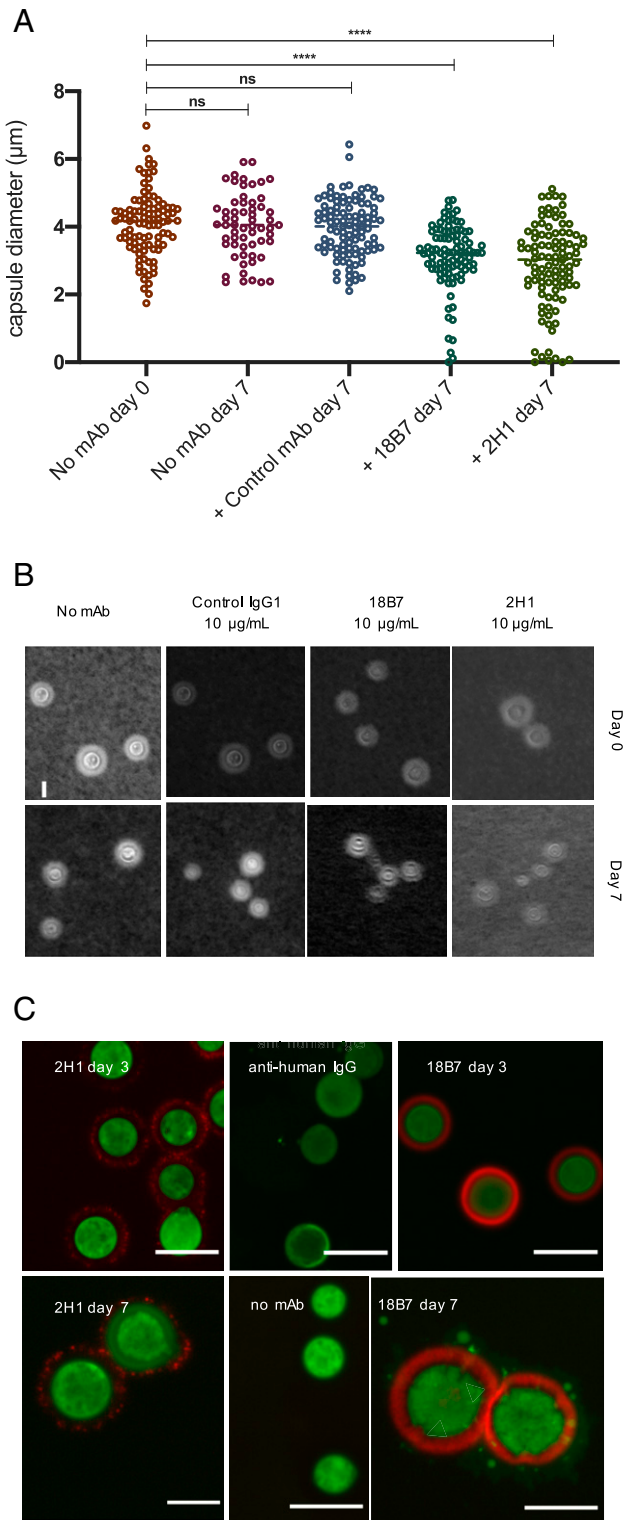

Fig. 6. Cells incubated with catalytic Abs have reduced capsule diameter, impaired cellular integrity, and the appearance of reducing glycans in the capsule from polysaccharide hydrolysis. (*A*) Heat-killed *C. neoformans* cells were incubated with 18B7, 2H1, a control IgG_1 Ab and no Ab for 7 d. Capsule measurements revealed a statistically significant (ordinary one-way ANOVA) decrease in mean capsule diameter when incubated with 18B7 or 2H1 but not in control experiments. Each group contained at least 100 capsule measurements (****$P < 0.0001$; ns, not significant). (*B*) Images of heat-killed fungal cells under each Ab condition at both day 0 and day 7. India ink stain allows visualization of capsule diameter. (Scale bar, 10 μm.) (*C*) Fluorescent microscopy of heat-killed *C. neoformans* cells incubated with 18B7, 2H1, anti-human IgG, or no antibody (no mAb) and imaged on days 3 and 7. An aminooxy probe was used to visualize the change in capsule architecture after exposure to catalytic Abs over time (green) and capsule shown in red (goat anti-mouse IgG FITC). (Scale bars, 5 μm.)

hypermutation and subsequent selection, since acetylated structures are more hydrophobic and contain more hydrogen bond acceptors for interactions with B cell receptors, which leads to less transient Ab-glycan interactions.

The validity of the FRET assay in reporting polysaccharide cleavage was confirmed by capsule measurement experiments and fluorescence microscopy with both experiments, suggesting the capsule and cryptococcal cell surface undergo changes when exposed to catalytic mAbs 2H1 and 18B7. While the biological importance of this effect is yet to be fully resolved—and we urge caution—it is still fascinating to consider. As the capsule is both immunosuppressive and antiphagocytic (53, 54), Ab-mediated hydrolysis of the capsule in vivo could have important immunological effects, decreasing the capsule diameter, revealing more immunogenic structures, and making phagocytosis more facile by macrophages, all of which could aid the immune system to fight cryptococcal infection. Our phagocytic index experiments suggest the catalytic activity of mAb 2H1 results in a tangible biological effect, but further work will be required to fully resolve this elusive quality in glycan-degrading Abs. We hope that our study raises questions over the ubiquity of catalytic Abs and what functional advantages might be given to an Ab with innate glycosidase activity against microbial or viral infection.

In summary, the use of two glycan FRET probes enabled the identification of four mAbs with innate catalytic activity toward glycans, of which mAb 2H1 was the most efficient. The role of mannose 6-*O*-acetylation in Ab recognition and catalysis was also demonstrated, by both the glycan microarrays studies and the observed kinetic differences in glycan FRET probe hydrolysis. Mass spectrometry analysis suggests mAb 2H1 operates in a manner that of a polysaccharide lyase enzyme, and examination of the crystal structure of mAb 2H1 revealed that the paratope of this Ab lacks classic glycosidase motifs. We surmise that if catalysis is achieved in the binding site, it is through a molecular mechanism yet to be discovered. The FRET probes accurately predicted catalytic activity on the native capsule, which was supported by fluorescence spectroscopy, capsule measurements, and an increased phagocytosis of cells exposed to catalytic Abs. The approach described here utilizing FRET probes could prove very useful for the identification of catalytic activity in other glycan-binding mAbs.

Methods

Microarray Printing. Glycan array printing closely followed published procedures (55). Microarrays were constructed by piezoelectric noncontact printing (sciFLEXARRAYER S3, Scienion) of the glycans on activated glass slides (Nexterion Slide H, Schott). Compounds (200 μM, 100 μM, 50 μM) were printed (drop volume ~300 pL, 6 drops per spot), in replicates of 5 in sodium phosphate (200 mM), pH 8.5 buffer with on each slide. Overnight the slides were incubated in a humidity chamber, and the remaining activated esters were blocked with ethanolamine (50 mM) in Tris (100 mM), pH 8.0. Next, slides were rinsed with MilliQ water, dried by centrifugation, and stored at 4 °C. Hybridization of arrays was performed as described previously (55). Briefly, printed slides were blocked in a humidity chamber at 26 °C for 2 h with 2% bovine serum albumin (BSA) in PBS (pH 7.4 with 50 mM ethanolamine), then washed three times for 2 min with PBS (pH 7.4, 0.1% Tween-20) (PBS-T) and once for 3 min with PBS.

Microarray Screening. Glycan array scanning followed published procedures (55). Primary anti-GXM mAbs or control Abs were prepared from stocks to the necessary concentration in 3% BSA in PBS-T. Biotinylated goat anti-mouse κ-chain Abs were used as secondary reagents for all primary Abs. Detection was performed with the streptavidin-conjugated SureLight P3 fluorophore (Cayman Chemical Company) at 5 μg/mL in PBS-T. Scanning was

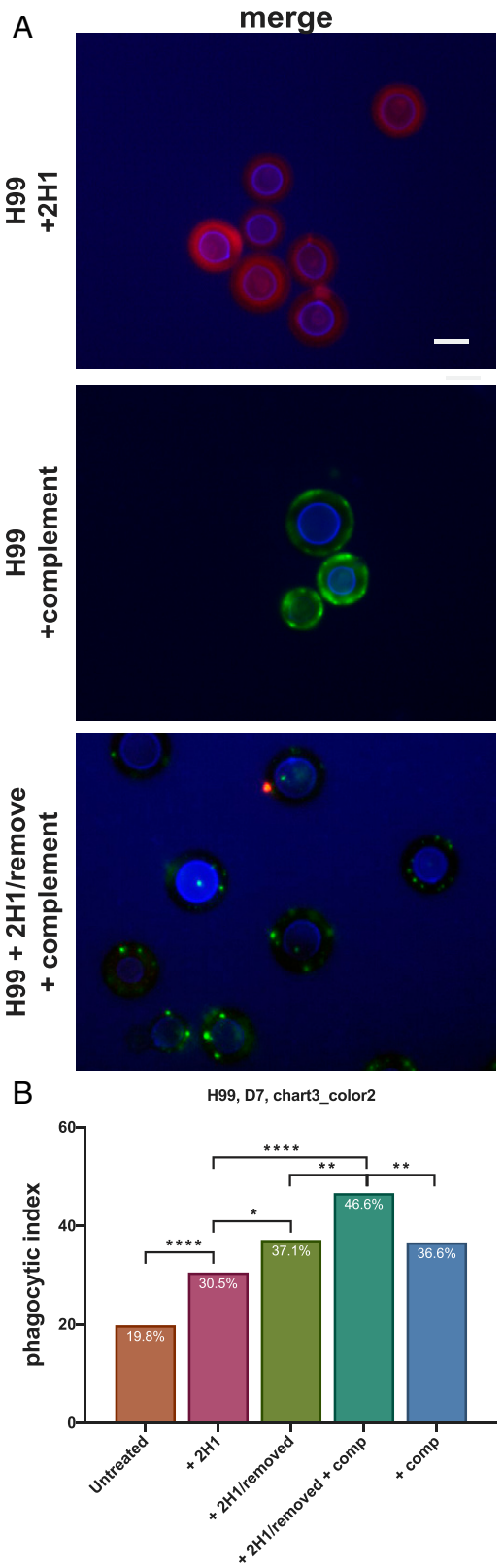

Fig. 7. Physiological importance of 2H1-mediated capsule damage. (*A*) The effects of complement deposition on the capsule of heat killed H99 *C. neoformans* was examined after incubation with 2H1 mAb or no Ab for 7 d. Cells were stained with specific fluorophore conjugated secondary Abs to visualize mAb and complement localization. (Scale bar, 6 μm.) (*B*) Phagocytic opsonization was measured for untreated H99 *C. neoformans* cells, cells treated with 2H1 mAb (with or without subsequent Ab removal) and guinea pig complement (with or without 2H1 treatment and removal). Statistically significant differences in phagocytic index where observed between untreated cells and all treatment conditions (χ^2 test for differences). The addition of complement to H99 *C. neoformans* cells treated with 2H1 yields a highly significant increase in phagocytic index compared to cells only treated with 2H1, suggested that altered complement deposition as a result of catalytic mAb remodeling of the capsule diminishes the antiphagocytic properties of the capsule (*$P < 0.5$; **$P < 0.01$; ***$P < 0.001$).

performed first with the primary Ab, then the secondary Ab, then the fluorophore, with washes between each step. All hybridization steps were performed using the Agilent eight-well gasket system in a humidity-controlled rotating hybridization oven at 26 °C for 1 to 2 h. Washes (3×) in Tris-buffered saline (pH 7.6, 0.1% Tween 20) (TBS-T) for 3 min and once for 3 min in TBS. Scanning was performed in an Agilent SureScan Dx microarray scanner with red wavelength emission detection. The data were processed on Mapix software. The mean fluorescent intensities (corrected for mean background) and SDs were calculated ($n = 6$). Data were fitted using Prism software (GraphPad Software, Inc). Bar graphs represent the mean ± SD for each compound.

FRET Probe Synthesis. Detailed protocols for the synthesis of novel compounds and their NMR characterization can be found in *SI Appendix*. Building blocks were synthesized as described previously (20, 24, 28, 56).

Growth Conditions. *C. neoformans* Serotype A strain H99 (American Type Culture Collection 208821), was grown for 48 h at 30 °C in capsule inducing media composed of: 10 mM $MgSO_4$, 29.3 mM KH_2PO_4, 13 mM glycine, 3 μM thiamine-HCl, and adjusted to pH 5.5 and supplemented with 15 mM dextrose.

Kinetic Experiments. FRET experiments were completed as reported by Bowen et al. (4) Using a SpectraMax M5 microplate reader (Molecular Devices), at 37 °C. An excitation wavelength of 320 nm, an emission wavelength of 405 nm, and an emission cutoff filter of 325 nm.

Molecular Modeling. GLYCAM carbohydrate builder was used to construct ligands and autodock vina for Ab-docking studies, both of which can be accessed at http://glycam.org (37–39). PyMOL was used for visualization and figure creation.

mAb Preparation. The 3E5-IgG_3 and 3E5-IgG_1 have been described previously (57, 58). mAb 18B7 and 2H1, were obtained as previously described (17, 59). The murine mAbs were purified by protein A or G affinity chromatography (Pierce) from hybridoma cell culture supernatants and concentrated and buffer exchanged against 0.1 M Tris·HCl pH 7.4. mAb concentration was determined by OD_{280} measurement.

Capsule Digestion Experiments. *C. neoformans* cultures were grown to stationary phase under capsule-inducing conditions in minimal media (2 d). Starting culture conditions were complete in Sabouraud medium. Cells were collected and heat-killed at 60 °C for 1 h. Complete killing was confirmed by plating on solid Sabouraud medium. Heat-killed cells were washed five times with PBS to remove any soluble polysaccharide and cells were collected by ultracentrifugation (4,000 × *g*, 5 min, 4 °C). Washed cells were suspended in a volume of PBS, which was divided equally between the four capsule digestion experiments: No mAb, control mAb (MOPC-31C, Sigma), 18B7, 2H1. All Ab incubations were carried out at 10 μg/mL. Each sample was diluted with PBS, pH 7.0, to a final volume of 2 mL and a concentration of 10^6 heat-killed cells per milliliter. Samples were then incubated at 37 °C with agitation. *C. neoformans* capsules were visualized at day 0 and at day 7 under light microscopy, by mixing 2 μL of India ink with 6 μL of cells. Images were taken with an Olympus AX 70 microscope. Capsule measurements were completed (Fiji, NIH) and compared to day 0 and day 7 (no mAb). Statistical analysis (ordinary one-way ANOVA) was performed in GraphPad Prism (Version 8, GraphPad Software).

Immunofluorescence Microscopy. As previously reported (43), H99 *C. neoformans* cells were grown inoculated in Sabouraud dextrose medium for 2 d and then transferred to capsule inducing minimal media for 3 d. Cells were then heat-killed at 60 °C for 1 h and incubated with the catalytic Ab 2H1 (10 μg/mL) for 7 d. Samples were taken at time points indicated in figures. Cells were stained with the reducing-end hydroxylamine fluorescent probe

(2.5 μM), 18B7 (10 μg/mL), or Complement [20% (wt/vol)]. For indicated samples 2H1 was removed after the indicated incubation using Gentle Ag/Ab Elution Buffer, pH 6.6 (Pierce Bioscience). Samples were incubated with the indicated probe in blocking solution (1% BSA) overnight at 30 °C in the dark. Cells were pelleted and washed to remove excess probe, three times in PBS plus 1% BSA. Goat anti-mouse anti-IgG1 secondary Ab—TRITC, goat anti-Complement C3 polyclonal—FITC, or directly conjugated IgG1 18B7-Alexa Fluor 594 conjugate were added at 1 μg/mL for 1 h, at 37 °C. After incubation cells were again washed three times with PBS plus 1% BSA. Uvitex2B was added to cells to stain the *C. neoformans* cell wall at a 1:10,000 dilution. Cells were then washed three times in PBS plus 1% BSA. Cells were mounted on slides at 1×10^6 cells per milliliter with Pro-Long Gold mounting solution (Molecular Probes). Channel exposures were: FITC (800 ms; excitation/emission 498/516 nm), TRITC (600 ms; excitation/emission 540/580 nm), and DAPI (50 ms; excitation/emission 350/450 nm). Images were collected with an Olympus AX70 microscope, photographed with a QImaging Retiga 1300 digital camera using the QCapture Suite V2.46 software (QImaging), and processed with ImageJ from Fiji (NIH).

Phagocytic Index Assay. Phagocytosis was measured as previously reported (60). Briefly, harvested and matured mouse BMDMs were plated at 5×10^5 cells/mL ~18 h prior to experiment. HK H99 *C. neoformans* cells incubated 7 d with, or without 2H1 Ab were harvested. 2H1 mAb was removed by adding gentle Ag/Ab elution buffer (pH 6.6) and incubating shaking at 37 °C for 2 h, then washing cells three times with TBS. 18B7 or Complement were added and incubated for 20 min prior to the addition of *C. neoformans* to the BMDMs. *C. neoformans* was added at a multiplicity of infection (MOI) of 3:1 to seeded macrophages and incubated for 2 h at 37 °C to allow for phagocytosis to occur. Cultures were gently washed 2× with BMDM media to remove nonphagocytosed *C. neoformans*. Cultures were visualized on a Carl Zeiss LSM 780 confocal microscope with a 403, 1.4 numerical aperture Plan Apochromat oil-immersion differential interference contrast objective and a spectral gallium arsenide phosphide detector in an enclosed chamber at 20× Brightfield. Acquisition parameters, shutters, and focus were controlled by ZEN Black software (Carl Zeiss).

Data Availability. All study data are included in the article and supporting information.

ACKNOWLEDGMENTS. We thank Dr. Yannick Ortin and Dr. Jimmy Muldoon for NMR and mass spectrometry support. C.J.C. was funded by Irish Research Council postgraduate Award GOIPG/2016/998. M.P.W. was supported in part by NIH Grant AI007417. A.C. was supported in part by NIH Grants AI052733-16, AI152078-01, and HL059842-19. S.O. was supported by Science Foundation Ireland Award 13/IA/1959.

1. A. Casadevall, Climate change brings the specter of new infectious diseases. *J. Clin. Invest.* **130**, 553–555 (2020).
2. A. Casadevall, E. Dadachova, L. A. Pirofski, Passive antibody therapy for infectious diseases. *Nat. Rev. Microbiol.* **2**, 695–703 (2004).
3. P. Wentworth *et al*., Antibody catalysis of the oxidation of water. *Science* **293**, 1806–1811 (2001).
4. A. Bowen, M. P. Wear, R. J. B. Cordero, S. Oscarson, A. Casadevall, A monoclonal antibody to Cryptococcus neoformans glucuronoxylomannan manifests hydrolytic activity for both peptides and polysaccharides. *J. Biol. Chem.* **292**, 417–434 (2017).
5. A. Janda *et al*., Variable region identical IgA and IgE to Cryptococcus neoformans capsular polysaccharide manifest specificity differences. *J. Biol. Chem.* **290**, 12090–12100 (2015).
6. A. Janda, E. Eryilmaz, A. Nakouzi, D. Cowburn, A. Casadevall, Variable region identical immunoglobulins differing in isotype express different paratopes. *J. Biol. Chem.* **287**, 35409–35417 (2012).
7. C. D. Gutsche, Catalysis in chemistry and enzymology. *Science* **168**, 1080–1081 (1970).
8. B. Mets *et al*., A catalytic antibody against cocaine prevents cocaine's reinforcing and toxic effects in rats. *Proc. Natl. Acad. Sci. U.S.A.* **95**, 10176–10181 (1998).
9. P. G. Schultz, Catalytic antibodies. *Angew. Chem. Int. Ed. Engl.* **28**, 1283–1295 (1989).
10. B. J. Park *et al*., Estimation of the current global burden of cryptococcal meningitis among persons living with HIV/AIDS. *AIDS* **23**, 525–530 (2009).
11. S. K. Chow, A. Casadevall, Evaluation of Cryptococcus neoformans galactoxylomannan-protein conjugate as vaccine candidate against murine cryptococcosis. *Vaccine* **29**, 1891–1898 (2011).
12. S. Oscarson, M. Alpe, P. Svahnberg, A. Nakouzi, A. Casadevall, Synthesis and immunological studies of glycoconjugates of Cryptococcus neoformans capsular glucuronoxylomannan oligosaccharide structures. *Vaccine* **23**, 3961–3972 (2005).
13. A. Nakouzi, T. Zhang, S. Oscarson, A. Casadevall, The common Cryptococcus neoformans glucuronoxylomannan M2 motif elicits non-protective antibodies. *Vaccine* **27**, 3513–3518 (2009).
14. R. Cherniak, H. Valafar, L. C. Morris, F. Valafar, Cryptococcus neoformans chemotyping by quantitative analysis of 1H nuclear magnetic resonance spectra of glucuronoxylomannans with a computer-simulated artificial neural network. *Clin. Diagn. Lab. Immunol.* **5**, 146–159 (1998).
15. S. Sheng, R. Cherniak, Structure of the 13C-enriched O-deacetylated glucuronoxylomannan of Cryptococcus neoformans serotype A determined by NMR spectroscopy. *Carbohydr. Res.* **301**, 33–40 (1997).
16. R. Cherniak, J. B. Sundstrom, Polysaccharide antigens of the capsule of Cryptococcus neoformans. *Infect. Immun.* **62**, 1507–1512 (1994).
17. R. A. Larsen *et al*., Phase I evaluation of the safety and pharmacokinetics of murine-derived anticryptococcal antibody 18B7 in subjects with treated cryptococcal meningitis. *Antimicrob. Agents Chemother.* **49**, 952–958 (2005).
18. G. A. Nevinsky, V. N. Buneva, Catalytic antibodies in healthy humans and patients with autoimmune and viral diseases. *J. Cell. Mol. Med.* **7**, 265–276 (2003).
19. A. Bowen, M. Wear, A. Casadevall, Antibody-mediated catalysis in infection and immunity. *Infect. Immun.* **85**, e00202-17 (2017).
20. L. Guazzelli *et al*., A synthetic glycan array containing Cryptococcus neoformans glucuronoxylomannan capsular polysaccharide fragments allows the mapping of protective epitopes. *Chem. Sci. (Camb.)* **11**, 9209–9217 (2020).
21. A. Casadevall *et al*., Antibodies elicited by a Cryptococcus neoformans-tetanus toxoid conjugate vaccine have the same specificity as those elicited in infection. *J. Infect. Dis.* **165**, 1086–1093 (1992).
22. S. J. N. Devi *et al*., Cryptococcus neoformans serotype A glucuronoxylomannan-protein conjugate vaccines: Synthesis, characterization, and immunogenicity. *Infect. Immun.* **59**, 3700–3707 (1991).
23. L. Guazzelli, R. Ulc, S. Oscarson, Synthesis of benzyl protected β-D-GlcA-(1→2)-α-d-Man thioglycoside building blocks for construction of Cryptococcus neoformans capsular polysaccharide structures. *Carbohydr. Res.* **389**, 57–65 (2014).
24. L. Guazzelli, R. Ulc, L. Rydner, S. Oscarson, A synthetic strategy to xylose-containing thioglycoside tri- and tetrasaccharide building blocks corresponding to Cryptococcus neoformans capsular polysaccharide structures. *Org. Biomol. Chem.* **13**, 6598–6610 (2015).
25. P. J. Garegg, L. Olsson, S. Oscarson, Synthesis of oligosaccharides corresponding to structures found in capsular polysaccharides of crytococcus neoformans. Part 1. *J. Carbohydr. Chem.* **12**, 955–967 (1993).
26. P. J. Garegg, L. Olsson, S. Oscarson, Synthesis of oligosaccharides corresponding to structures found in capsular polysaccharides of Cryptococcus neoformans. Part 3. Two regioselectively acetylated tetrasaccharides. *J. Carbohydr. Chem.* **16**, 973–981 (1997).
27. M. Alpe, S. Oscarson, P. Svahnberg, Synthesis of Cryptococcus neoformans capsular polysaccharide structures. IV. Construction of thioglycoside donor blocks and their subsequent assembly. *J. Carbohydr. Chem.* **22**, 565–577 (2003).
28. C. Crawford, S. Oscarson, Optimized conditions for the palladium-catalyzed hydrogenolysis of benzyl and naphthylmethyl ethers: Preventing saturation of aromatic protecting groups. *Eur. J. Org. Chem.* **2020**, 3332–3337 (2020).
29. C. J. Crawford, S. Oscarson, Convergent total synthesis of Cryptococcus neoformans serotype B capsule repeating motif. *Carbohydr. Res.* **497**, 108150 (2020).
30. P. Fügedi, P. J. Garegg, A novel promoter for the efficient construction of 1,2-trans linkages in glycoside synthesis, using thioglycosides as glycosyl donors. *Carbohydr. Res.* **149**, 9–12 (1986).
31. C. Crawford *et al*, Clues to a Pd/C catalyst's efficiency can be found on its surface: Identification of an efficient catalyst for the global hydrogenolysis of ether protecting groups. *ChemRxiv* [Preprint] (2020). https://doi.org/10.26434/chemrxiv.12793634.v1 (Accessed 15 January 2021).
32. J. Mukherjee, A. Casadevall, M. D. Scharff, Molecular characterization of the humoral responses to Cryptococcus neoformans infection and glucuronoxylomannan-tetanus toxoid conjugate immunization. *J. Exp. Med.* **177**, 1105–1116 (1993).
33. R. Yuan, A. Casadevall, G. Spira, M. D. Scharff, Isotype switching from IgG3 to IgG1 converts a nonprotective murine antibody to Cryptococcus neoformans into a protective antibody. *J. Immunol.* **154**, 1810–1816 (1995).
34. S. A. K. Jongkees, S. G. Withers, Unusual enzymatic glycoside cleavage mechanisms. *Acc. Chem. Res.* **47**, 226–235 (2014).
35. H. J. Rozeboom *et al*., Crystal structure of α-1,4-glucan lyase, a unique glycoside hydrolase family member with a novel catalytic mechanism. *J. Biol. Chem.* **288**, 26764–26774 (2013).
36. A. C. M. Young, P. Valadon, A. Casadevall, M. D. Scharff, J. C. Sacchettini, The three-dimensional structures of a polysaccharide binding antibody to Cryptococcus neoformans and its complex with a peptide from a phage display library: Implications for the identification of peptide mimotopes. *J. Mol. Biol.* **274**, 622–634 (1997).
37. S. Makeneni, D. F. Thieker, R. J. Woods, Applying pose clustering and MD simulations to eliminate false positives in molecular docking. *J. Chem. Inf. Model.* **58**, 605–614 (2018).
38. A. K. Nivedha, D. F. Thieker, S. Makeneni, H. Hu, R. J. Woods, Vina-Carb: Improving glycosidic angles during carbohydrate docking. *J. Chem. Theory Comput.* **12**, 892–901 (2016).
39. A. K. Nivedha, S. Makeneni, B. L. Foley, M. B. Tessier, R. J. Woods, Importance of ligand conformational energies in carbohydrate docking: Sorting the wheat from the chaff. *J. Comput. Chem.* **35**, 526–539 (2014).
40. V. Spiwok, CH/π interactions in carbohydrate recognition. *Molecules* **22**, 1038 (2017).
41. D. L. Zechel, S. G. Withers, Glycosidase mechanisms: Anatomy of a finely tuned catalyst. *Acc. Chem. Res.* **33**, 11–18 (2000).
42. P. Bule *et al*., Inverting family GH156 sialidases define an unusual catalytic motif for glycosidase action. *Nat. Commun.* **10**, 4816 (2019).

43. C. J. Crawford *et al*., Exploring *Cryptococcus neoformans* capsule structure and assembly with a hydroxylamine-armed fluorescent probe. *J. Biol. Chem.* **295**, 4327–4340 (2020).
44. O. Zaragoza, A. Casadevall, Monoclonal antibodies can affect complement deposition on the capsule of the pathogenic fungus Cryptococcus neoformans by both classical pathway activation and steric hindrance. *Cell. Microbiol.* **8**, 1862–1876 (2006).
45. G. Y. Yang *et al*., A FRET probe for cell-based imaging of ganglioside-processing enzyme activity and high-throughput screening. *Angew. Chem. Int. Ed. Engl.* **54**, 5389–5393 (2015).
46. S. Cecioni, D. J. Vocadlo, Carbohydrate Bis-acetal-based substrates as tunable fluorescence-quenched probes for monitoring exo-glycosidase activity. *J. Am. Chem. Soc.* **139**, 8392–8395 (2017).
47. K. Sano *et al*., Fluorescence quenching-based assay for measuring Golgi endo-α-Mannosidase. *Chem. Asian J.* **14**, 1965–1969 (2019).
48. H. Oka, T. Koyama, K. Hatano, K. Matsuoka, Synthetic studies of bi-fluorescence-labeled maltooligosaccharides as substrates for α-amylase on the basis of fluorescence resonance energy transfer (FRET). *Bioorg. Med. Chem.* **20**, 435–445 (2012).
49. J. C. Sistla *et al*., Polymeric fluorescent heparin as one-step FRET substrate of human heparanase. *Carbohydr. Polym.* **205**, 385–391 (2019).
50. A. Guerry *et al*., Aniline-catalyzed reductive amination as a powerful method for the preparation of reducing end-"clickable" chitooligosaccharides. *Bioconjug. Chem.* **24**, 544–549 (2013).
51. M. M. Kuttel, A. Casadevall, S. Oscarson, *Cryptococcus neoformans* capsular GXM conformation and epitope presentation: A molecular modelling study. *Molecules* **25**, 2651 (2020).
52. R. Vij, C. Danchik, C. Crawford, Q. Dragotakes, A. Casadevall, Variation in cell surface hydrophobicity among Cryptococcus neoformans strains influences interactions with amoebas. *MSphere* **5**, e00310-20 (2020).
53. M. Del Poeta, Role of phagocytosis in the virulence of Cryptococcus neoformans. *Eukaryot. Cell* **3**, 1067–1075 (2004).
54. O. Zaragoza *et al*., The capsule of the fungal pathogen Cryptococcus neoformans. *Adv. Appl. Microbiol.* **68**, 133–216 (2009).
55. M. Kilcoyne *et al*., Construction of a natural mucin microarray and interrogation for biologically relevant glyco-epitopes. *Anal. Chem.* **84**, 3330–3338 (2012).
56. L. Guazzelli, R. Ulc, S. Oscarson, Synthesis of a glucuronic acid-containing thioglycoside trisaccharide building block and its use in the assembly of Cryptococcus neoformans capsular polysaccharide fragments. *ChemistryOpen* **4**, 729–739 (2015).
57. M. Torres, N. Fernandez-Fuentes, A. Fiser, A. Casadevall, Exchanging murine and human immunoglobulin constant chains affects the kinetics and thermodynamics of antigen binding and chimeric antibody autoreactivity. *PLoS One* **2**, e1310 (2007).
58. T. K. Dam, M. Torres, C. F. Brewer, A. Casadevall, Isothermal titration calorimetry reveals differential binding thermodynamics of variable region-identical antibodies differing in constant region for a univalent ligand. *J. Biol. Chem.* **283**, 31366–31370 (2008).
59. A. Casadevall *et al*., Characterization of a murine monoclonal antibody to Cryptococcus neoformans polysaccharide that is a candidate for human therapeutic studies. *Antimicrob. Agents Chemother.* **42**, 1437–1446 (1998).
60. S. C. Tucker, A. Casadevall, Replication of Cryptococcus neoformans in macrophages is accompanied by phagosomal permeabilization and accumulation of vesicles containing polysaccharide in the cytoplasm. *Proc. Natl. Acad. Sci. U.S.A.* **99**, 3165–3170 (2002).
61. A. Varki *et al*., Symbol nomenclature for graphical representations of glycans. *Glycobiology* **25**, 1323–1324 (2015).